Oxygen Monitor to Study Vascularization of Medical Devices

Avid Najdahmadi[1*], Rachel Gurlin[2*], Mellonie Zhang[2], Jonathan RT Lakey[2,3], Elliot Botvinick[1,2,3]

[1] *Department of Materials Science and Engineering, University of California Irvine, Irvine, USA*

[2] *Department of Biomedical Engineering, University of California Irvine, Irvine, USA*

[3] *Department of Surgery, University of California Irvine, Irvine, USA*

* These authors contributed equally

Abstract:

Prevascularized medical devices can improve cell therapy. Such devices may replace whole organ transplantation with hosting only the necessary therapeutic cells. We have developed a noninvasive optical technology to study the vascularization into such medical devices. In our technique, oxygen partial pressure within a device is monitored by Oxygen Sensitive Tubes (OSTs), comprising oxygen permeable silicone tubing with inner luminal surfaces coated by an oxygen-sensitive porphyrin dye. OSTs were placed within a PDMS device and transplanted into the subcutaneous space of athymic nude mice. An optical probe placed over the skin excites the OSTs with a pulse of light and detects the luminescent lifetime of emitted light, which is uniquely related to oxygen partial pressure. Furthermore, we developed a Dynamic Inhalation Gas Test (DIGT) to determine the oxygen transport rate between the microvasculature and the device. DIGT works by monitoring oxygen partial pressure in a device following a step change in inhaled-gas oxygen content. We report DIGT oxygen dynamics measured intermittently over eight weeks. Our study shows DIGT dynamics are unique to each implant, supporting the important role of the host tissue response in the availability of oxygen over time.

CrossMark

INTRODUCTION:

Cell transplantation approaches have been emerging as an alternative to whole organ transplantation for replacement of dysfunctional organs [1]. For example, in the case of type 1 diabetes, insulin-producing cells within pancreatic islets are destroyed by the immune system, which results in unchecked glycemic control [2]. Currently, the most common method of treatment is daily injection of insulin, which is not a cure, and can cause secondary microvascular conditions [3]. One promising approach as an alternative to whole pancreas transplantation is isolation and transplantation of insulin-producing pancreatic islets [4]. However, the main limitation of such an approach is the limited supply of human donor cells, which necessitates new approaches such as xenotransplantation, ultimately resulting in rejection of the transplanted islets by the recipient's immune system, and therefore necessitating lifelong immunosuppression drug therapy[5]. Various tissue engineering techniques have been used to address this problem. In one strategy, the pancreatic islets are encapsulated within an implantable hydrogel capsule, medical device or bioartificial organ [6,7]. Such devices must maintain functionality of the pancreatic islets through sustained permeability to nutrients such as glucose, oxygen, and secreted insulin [8-11]. The tissue foreign body response may result in formation of a fibrous capsule surrounding the device and restriction of molecular transport with host vasculature. The severity of the foreign body response varies with implantation site. While the subcutaneous space is advantageous over deeper body cavities due to its ease of access for device implantation and retrieval, it is sparsely vascularized. Thus, the subcutaneous space provides low levels of oxygen, thereby increasing the risk of hypoxia, which results in the loss of functionality and death of the implanted cells [12-15]. As a result, it is necessary to allow oxygen-carrying vasculature to grow into the medical device, shortening diffusional distances and increasing oxygen transport to the transplanted cells. This prevascularization process can be achieved through different strategies such as administration of angiogenic factors, which would require additional regulatory considerations [16], or use of microporous structures known to promote tissue integration, which while effective, face limitations due to variations between pores geometries [17]. An alternative approach is the use of devices with specific internal geometries designed to allow the vasculature to grow into the implanted device, as we have done previously [18,19]. Ultimately, success of these approaches demands an oxygen rich environment to be established prior to introducing therapeutic cells.

Here we study the vascularization and oxygenation of our previously developed polydimethylsiloxane (PDMS) thin-sheet device [18]. These PDMS sheets are designed to house transplanted cells arranged in single file within microfluidic channels. These channels are connected with a repeating array of windows, which open into long slits passing through the sheet (Fig.1). Prior to implantation, device channels are plugged by oxygen sensitive tubes (OSTs) comprising a phosphorescent porphyrin dye film coating the inner surface of oxygen-permeable tubing. OSTs allow for in situ monitoring of device oxygenation as tissue grows into the slits and windows. Such monitoring will indicate if and when a device is well oxygenated. OSTs can then be removed by a small incision through the skin, leaving behind empty channels to be filled with therapeutic cells. In this current study, device oxygenation and transport is monitored for eight weeks following implantation in the subcutaneous space of athymic nude mice.
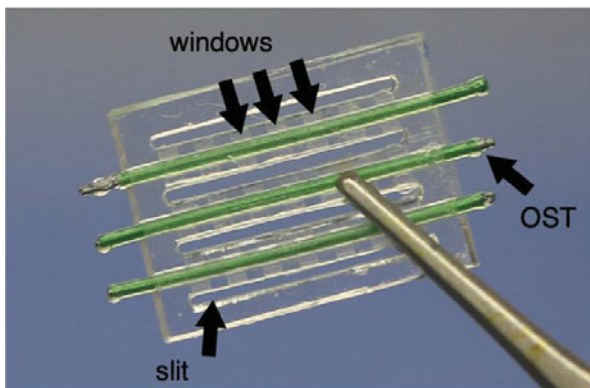
Figure 1. Thin device is made of PDMS with features of: slits passing through the thickness, OSTs passing through channels, and windows within the thickness of the sheet connecting channels to slits.

MATERIALS AND METHODS

PDMS Device

A typical device is shown in Figure 1, comprising slits, channels, and windows (to connect slits and channels). PDMS (Sylgard® 184 Silicone Elastomer Kit, USA) devices are fabricated as previously described by Gurlin *et al.* [18]. Each device is assembled from a 'ceiling' and 'floor' piece. The floor contains all features of the device while the ceiling is a solid sheet of silicone. Ceiling and floor pieces are treated in a plasma cleaner (Harrick Plasma, Ithaca, USA) and bonded together. Slits are cut through the ceiling piece to align with slits in the floor. Each fabricated PDMS device has dimensions 10 x 13 x 1.2 mm^3 comprising a parallel array of four slits (500 μm width), three channels with cross-sectional dimensions 700 x 700 μm^2, and windows connecting slits with channels. Windows have cross-sectional dimensions 100 x 750 μm^2. The walls between each of the slits and channels are 500 μm thick.

Oxygen Sensitive Tubes (OSTs)

OSTs were fabricated as previously described [20]. OSTs comprise oxygen-sensitive dye that coats the inner wall of a biocompatible, oxygen-permeable silicone tube. The oxygen-sensitive dye, platinum (II)-meso-tetra (4-fluorophenyl) tetrabenzoporphyrin (PtTPTBPF), has peak absorption at 430 and 614 nm and peak emission at 733 nm (Frontier Scientific, USA). The dye was mixed with polystyrene (MW 2500, Sigma, USA) and dissolved in chloroform (Sigma, USA) at a 1:15:225 ratio of dye to polystyrene to chloroform. The dye solution was flushed through silicone tubes (BTSIL-025, Instech Laboratories, USA) five times to form homogeneous films of PtTPTBPF along the inner surface. The oxygen-permeable silicone tubes had inner and outer diameters of 0.31 mm and 0.64 mm, respectively. Coated tubes were stored for 24 hours in a dark, well-ventilated environment at 24℃ to allow complete chloroform evaporation. To increase mechanical stability, 24-gauge stainless-steel wires (Kanthal A1, Sweden) were inserted into each tube. The tubes containing wires were cut into 13

mm sections to match the length of the PDMS devices. Finally, the ends of each tube segment were sealed with medical grade silicone adhesive (MED-1000, Nusil, USA) and cured at room temperature in a dark environment for two days. One OST was placed into each channel of the PDMS devices, and the fully assembled devices were sterilized in 70% alcohol for 12 hours.

Oxygen Monitor

The oxygen monitor was fabricated as previously described by Najdahmadi *et al.* [20] to excite and then measure light emission from OSTs. It is designed to be placed on the surface of the skin aligned to an implanted device. The monitor consists of a custom printed circuit board (PCB) that houses a silicon photodetector (FDS100, Thorlabs, USA) and two red light emitting diodes (LEDs) having central emission wavelengths of 617 nm (Luxeon Rebel, Netherlands). An optical bandpass filter is placed before the photodetector to filter out LED emission. For each measurement, LEDs are modulated by a 97 Hz square wave (25 cycles) at 1% duty cycle (100 μs on, 10,200 μs off) to excite the oxygen sensitive dye. Photocurrent is converted to voltage by an operational amplifier and sampled for 200 microseconds at a frequency of 500 kHz with a myRIO Data Acquisition Module (National Instruments, USA). Data acquisition timing is controlled by a custom LabVIEW code (National Instruments, USA). Detector signals were background subtracted and fit to an exponential decay to determine the luminescent lifetime constant τ. Curve fitting is implemented by the nonlinear least squares regression function in MATLAB (MathWorks, USA).

OST Calibration

OSTs were calibrated in a resealable glass chamber placed adjacent to the oxygen monitor. Chambers were filled serially with mixtures of N_2 and O_2 at atmospheric pressure, having PO_2 of 160, 76, 38 , and 15.2 mmHg, as well 0 mmHg (100% Ar gas). τ was measured for each gas mixture to generate a calibration curve. OSTs were then matched by their calibration curves into groups of three and inserted into PDMS devices. Each device was then calibrated prior to implantation.

Animal Study

All described animal procedures were approved by the University of California Institutional Animal Care and Use Committee at the University of Irvine (IACUC # 2008-2850). PDMS devices were implanted in the subcutaneous space of eight-week old male athymic nude mice (n=5) (Envigo) for eight weeks. A small incision (~15 mm) through the dorsal skin was created by sterile scissors and a subcutaneous pocket was created by blunt dissection. One device per animal was placed into the pocket using tweezers and the dorsal incision was secured with surgical clips. The animals received ibuprofen, between 50 and 80 mg/kg, via drinking water for 2 days following surgery. The animals were housed at a University of California, Irvine animal facility and maintained under 12-hour light/dark cycles with *ad libitum* access to water and standard chow. Animals were monitored daily until devices were explanted.

Dynamic Inhaled Gas Test (DIGT)

First, a mouse is anesthetized while breathing a gas mixture of 760 mmHg (100%) oxygen with 2-3% of isoflurane (Piramel Healthcare, United Kingdom). After

the animal is under full anesthesia, the gas is exchanged for a mixture of 152 mmHg (21%) oxygen with 1.5% isoflurane. The oxygen monitor is then placed on the skin of the mouse directly above the implanted PDMS device and measurements begin. After 100 measurements (spaced by 4.25 sec) the inhaled gas mixture is switched back to 760 mmHg PO_2 with isoflurane. Measurements are acquired every 4.25 seconds for a duration of 60 minutes.

<u>**Histological Analysis and Immunofluorescence Staining**</u>

Animals were euthanized at day 56. Devices were explanted and fixed in 10% phosphate buffered formalin for 24 hr. Samples were blocked on edge in paraffin, sectioned, stained for H&E, and imaged with a Nikon eclipse E800 microscope at 4× magnification using the Olympus cellSens Entry program. Tissues within each slit of the device (Fig. 1) were imaged at 20× magnification and images stitched together using Fiji. Stitched images for each slit were analyzed with a custom MATLAB code for manual tracing of blood vessels. The vessel area percentage and count were calculated as total vessel area or count divided by total slit-tissue area. In preparation for Immunohistochemical staining, sections were deparaffinized, rehydrated, and subjected to overnight incubation in 0.1 M Tris/HCl buffer, pH = 9 at 80°C. Sections were washed with PBS, permeabilized with 0.5% Triton X-100, and blocked with 5% donkey serum (Jackson ImmunoResearch, USA) for 1 hr at room temperature. After blocking, slides were incubated overnight at 4°C with 1:200 monoclonal rabbit anti-alpha smooth muscle actin (ab124964, Abcam) and 1:200 polyclonal goat anti-CD31 (sc-1506, Santa Cruz Biotechnology) in PBS with 5% donkey serum and 0.5% Triton X-100. Slides were washed with PBS and incubated with 1:500 AlexaFluor 488 donkey anti-rabbit (Life Technologies, Cambridge, UK) and 1:400 AlexaFluor 594 donkey anti-goat (Jackson ImmunoResearch). DAPI (1:3000, Invitrogen) counterstaining was also performed. Images were acquired with an Olympus IX-83 fluorescence microscope with a 20× magnification air objective and an Orca R2 camera (Hamamatsu Photonics, Japan) through Micro Manager and stitched together using Fiji.

<u>**Statistics**</u>

Statistical analyses were performed in GraphPad Prism (version 7.0d; GraphPad Software, Inc, USA) and MATLAB. Shapiro-Wilk normality test was performed to test the data for normality. For DIGTs , the nonparametric Friedman test followed by post-hoc Dunn's multiple comparisons tests were used to detect differences amongst groups. For vessel area and density data, the nonparametric Kruskal-Wallis test with post-hoc Dunn's multiple comparison tests were used to compare individual devices. p-values < 0.05 were considered significant. The data is presented as median ± interquartile range.

RESULTS:

A prototypical device loaded with three OSTs is shown in Fig. 1. These devices were calibrated as described above with typical data shown in Fig. 2A. A second-order polynomial calibration curve is fit to data (Fig. 2B) where τ_0 is luminescent lifetime in an oxygen-free environment.
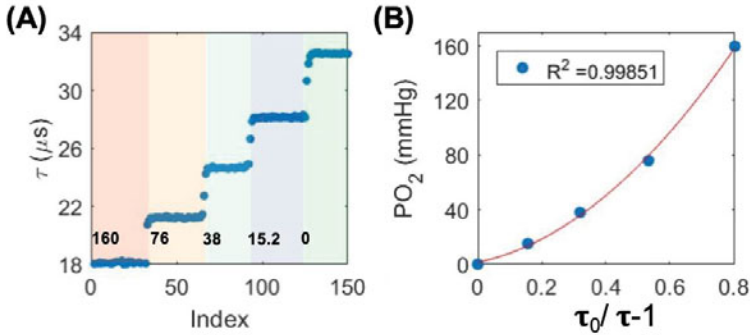
Figure 2. OST Calibration of single device containing OSTs (e.g. Fig.1) placed in a glass chamber. (A) Serial lifetime value for a range of PO_2 (160, 76, 38, 15.2, 0) mmHg. (B) Second-order polynomial curve fit where τ_0 is lifetime in an oxygen-free environment, and τ is the average plateau value of τ in (A).

Alignment between the oxygen monitor and an implanted device is a challenge during *in vivo* experiments, justifying the use of lifetime, and not luminescent intensity alone, for calibrated signals. An experiment was designed such that during calibration the oxygen monitor is iteratively translated relative to the device along a direction parallel to the OSTs. It is observed that signal amplitude (Fig. 3A) is quite sensitive to translation of the oxygen monitor whereas τ is insensitive, even after 1 cm translation, which is roughly the length of the OSTs (Fig. 3B). While there is observable sensitivity to translation at PO_2 of 160 mmHg, this value is super-physiological, whereas 75 and 15.2 mmHg are physiological. These data indicate precise probe placement is not required during *in vivo* oxygen measurements.
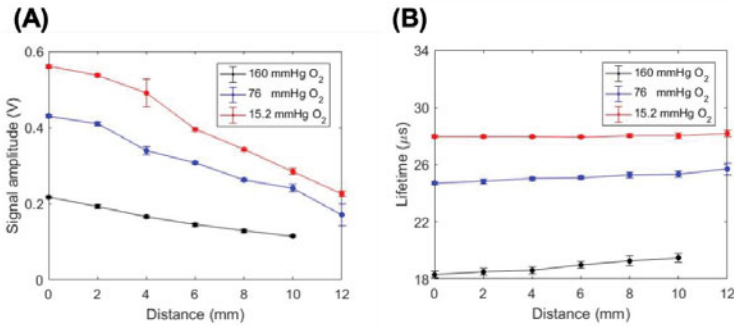

Figure 3. Lifetime measurements are insensitive to probe positioning over a distance of 1 cm. Movement of the probe shows that (A) misalignment of the probe relative to the OSTs reduces emission intensity at all three PO_2 levels (160, 76 and 15.2 mmHg). However, the calculated average lifetime (B) values remain constant out to 10 mm.

996

DIGT measurements were performed on days 3, 7, 14, 21, 28, 35, 42, 49 and 56 post implantation. A sample DIGT plot is shown in Fig. 4A. The time period during which the animal is breathing 760 mmHg PO_2 is indicated by the green boxes. DIGT experiments are compared by the parameter R (mmHg/min) as defined in Fig. 4A. R is greatest on day 3 and trends downwards overtime (Fig. 3B) indicated a lessening in oxygen availability. Differences in R were detected across days (p=0.0009) and the Dunn's multiple comparisons test found significant decreases in R between days 3 and 35 as well as days 7 and 35.
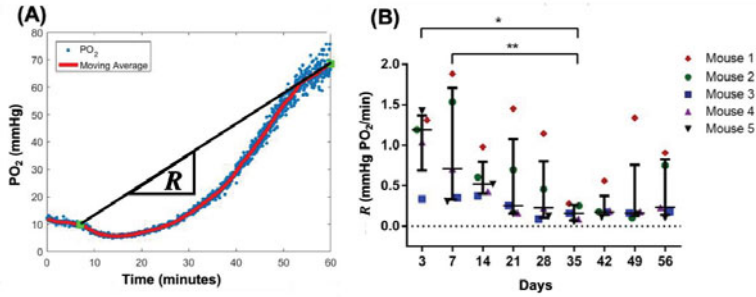

Figure 4. Oxygen dynamics measured by DIGTs over an 8 weeks period. (A) Prototypical dynamic inhaled gas test (DIGT). (B) R measured at timepoints spanning 56 days.

Figure 5 summarizes histological analyses of tissue grown into the slits (day 56). A cross-sectional field from one device is shown in Fig. 5A, with a higher magnification image of a single slit in Fig. 5B. Both images indicate tissue growth and vascular infiltration into the slits, confirmed by immunostaining for CD31 and αSMA, markers of vascular endothelial cells and pericytes, respectively (Fig. 5C). Quantification of vessel area and density indicates no differences between the devices (Fig. 5D).
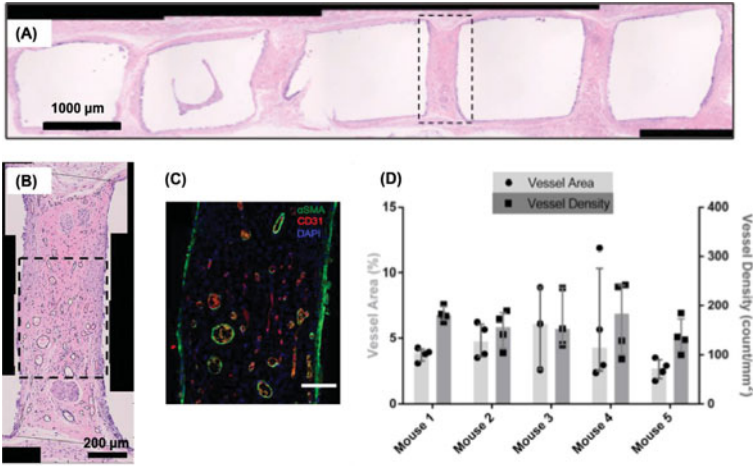
Figure 5. Histology of slit tissue within a PDMS device with surrounding tissue after eight weeks of implantation. (A) H&E staining of a vertical slice through a device. (B) Black outlies were hand drawn on H&E images to count vessels and their area. (C) Immunostaining for αSMA (green) and CD31 (red) shows a vascularized tissue within a slit. (D) Vessel count and area were not statistically different between mice (p=0.7)

DISCUSSION:

In this study we introduce a technique for noninvasive monitoring of dissolved oxygen within implanted medical devices. The technique utilizes an oxygen-sensitive porphyrin dye whose phosphorescence is sufficiently bright and not affected by background light, as is the case with fluorescent-dependent photonic sensors. Further, unlike fluorescence that has typical picosecond lifetime decay constants, PtTPTBPF lifetime constants are in the tens of microseconds. These two characteristics (brightness and long decay time) allow for phosphorescence lifetime measurements using relatively low-cost and 'slow' photodetection schemes, facilitating lifetime-decay detection, which is far less sensitive to motion, device-monitor alignment, and tissue optical properties as compared to time-integrated detection. And so, integration of technologies such as OSTs into devices allows for longitudinal and non-invasive monitoring of oxygen partial pressure, and provides insights into the changing microenvironment over long durations. Notably, DIGT experiments in this study show that upon inhalation of high levels of oxygen (760 mmHg), PO_2 within implanted devices increases over the course of one hour. We hypothesized the rate of change of PO_2 should be related to proximity of newly formed vasculature to OSTs, and therefore the state of vascularization. *In vitro* calibration shows OSTs respond quickly to changes in oxygen, reaching a new steady state following gas exchange in approximately ten seconds. Comparatively, DIGT dynamics occur on the time scale of tens of minutes, suggesting oxygen transport is a function of dissolved oxygen in the microvasculature as well as tissue composition. The eight week *in vivo* study shows slower oxygen transport on day 35 as compared to earlier timepoints, which suggests a decrease in vascularization and (or) increase is fibrotic tissue, which is the primary impedance to oxygen diffusion in the system. The exact

anatomy of slowing oxygen transport cannot be reported because this study was not designed to include a set of animals euthanized at each time point. However, histological analyses were conducted on day 56, for which R is not significantly different from day 35. Consequently, it may be reasonable to extrapolate day 56 histology to day 35. This histology shows sparse vascularization across all devices (animals) without significant differences in either vasculature density or vessel area. One obvious interpretation is that PDMS devices are not well integrated into the host and as a result, all devices show reduced oxygen transport after eight weeks in the subcutaneous space. Not surprisingly, R values are relatively large during the first week of implantation when the inflammatory response recruits new vessels to the site of each device thereby transiently elevating the local PO_2, however, as inflammation transitions into the foreign body response, fibroblasts will deposit new collagen and vessels resolve [21] slowing the transport of oxygen as reported by OSTs during a DIGT.

CONCLUSION

In summary, OSTs are a noninvasive photonic tool for measuring PO_2 within implanted devices. The developed OST and oxygen monitor technology is reliable, photostable, and insensitive to the position of the probe relative to the device. DIGT experiments were designed to rapidly increase PO_2 in the microvasculature as OSTs are monitored for the next hour to capture oxygen dynamics between the new vasculature, through the tissue and into each device. Metrics, such as R may be suitable as an indicator of device readiness with respect to oxygen availability to receive therapeutic cells. Our method may be a valuable tool for medical device development where effects of factors such as materials, fabrication, and geometry on device vascularization can be monitored longitudinally *in vivo*.

ACKNOWLEDGMENTS

REFERENCES

[1] R.S. Langer and J.P. Vacanti, Sci. Am. **280**, 86 (1999).
[2] J.-W. Yoon and H.-S. Jun, American Journal of Therapeutics **12**, 580 (2005).
[3] Am. J. Ophthalmol. **129**, 704 (2000).
[4] G.W. Burke, G. Ciancio, and H.W. Sollinger, Transplantation **77**, S62 (2004).
[5] T. Froud, C. Ricordi, D.A. Baidal, M.M. Hafiz, G. Ponte, P. Cure, A. Pileggi, R. Poggioli, H. Ichii, A. Khan, J.V. Ferreira, A. Pugliese, V.V. Esquenazi, N.S. Kenyon, and R. Alejandro, Am. J. Transplant **5**, 2037 (2005).
[6] J.H. Juang, S. Bonner-Weir, Y. Ogawa, J.P. Vacanti, and G.C. Weir, Transplantation **61**, 1557 (1996).
[7] A. Pileggi, R.D. Molano, C. Ricordi, E. Zahr, J. Collins, R. Valdes, and L. Inverardi, Transplantation **81**, 1318 (2006).
[8] P. de Vos, A.F. Hamel, and K. Tatarkiewicz, Diabetologia **45**, 159 (2002).
[9] A. Najdahmadi, J.R.T. Lakey, and E. Botvinick, MRS Advances **3**, 2399 (2018).
[10] J. Lakey, E. Botvinick, and A. Najdahmadi, Nanoscale Imaging, Sensing, and Actuation for Biomedical Applications XV (2018).
[11] P. de Vos, P. de Vos, M. Spasojevic, and M.M. Faas, Advances in Experimental Medicine and Biology 38 (2010).
[12] N. Sakata, T. Aoki, G. Yoshimatsu, H. Tsuchiya, T. Hata, Y. Katayose, S. Egawa, and M. Unno, Diabetes. Metab. Res. Rev. **30**, 1 (2014).
[13] A. Hakamivala, Y. Huang, Y. Chang, Z. Pan, A. Nair, J. Hsieh, and L. Tang, Advanced Biosystems **3**, 1900019 (2019).

[14] A. Nojoomi, E. Tamjid, A. Simchi, S. Bonakdar, and P. Stroeve, International Journal of Polymeric Materials and Polymeric Biomaterials 66, 105 (2017).

[15] A.R. Pepper, R. Pawlick, B. Gala-Lopez, A. MacGillivary, D.M. Mazzuca, D.J.G. White, P.M. Toleikis, and A.M. James Shapiro, Transplantation **99**, 2294 (2015).

[16] E.A. Phelps, K.L. Templeman, P.M. Thulé, and A.J. García, Drug Delivery and Translational Research **5**, 125 (2015).

[17] B.D. Ratner, Regen Biomater **3**, 107 (2016).

[18] R.E. Gurlin, M.T. Keating, S. Li, J.R. Lakey, S. de Feraudy, B.S. Shergill, and E.L. Botvinick, J. Tissue Eng. **8**, 2041731417691645 (2017).

[19] T.J. Thorson, R.E. Gurlin, E.L. Botvinick, and A. Mohraz, Acta Biomater. 94, 173 (2019).

[20] A. Najdahmadi, A.M Smink, P. de Vos, J.R.T. Lakey and E. Botvinick, Cell Transplantation (2020).

[21] M.G. Tonnesen, X. Feng, and R.A.F. Clark, Journal of Investigative Dermatology Symposium Proceedings **5**, 40 (2000).